Irregular Proton Injection to High Energies at Interplanetary Shocks

Domenico Trotta[1] , Timothy S. Horbury[1] , David Lario[2] , Rami Vainio[3] , Nina Dresing[3] , Andrew Dimmock[4] ,
Joe Giacalone[5] , Heli Hietala[6] , Robert F. Wimmer-Schweingruber[7] , Lars Berger[7] , and Liu Yang[7]

[1] The Blackett Laboratory, Department of Physics, Imperial College London, London SW7 2AZ, UK; d.trotta@imperial.ac.uk
[2] Heliophysics Science Division, NASA Goddard Space Flight Center, Greenbelt, MD 20771, USA
[3] Department of Physics and Astronomy, University of Turku, Finland
[4] Swedish Institute of Space Physics, Uppsala, Sweden
[5] Lunar and Planetary Laboratory, University of Arizona, Tucson, USA
[6] School of Physics and Astronomy, Queen Mary University of London, London E1 4NS, UK
[7] Institute of Experimental and Applied Physics, Kiel University, D-24118 Kiel, Germany

Abstract

How thermal particles are accelerated to suprathermal energies is an unsolved issue, crucial for many astrophysical systems. We report novel observations of irregular, dispersive enhancements of the suprathermal particle population upstream of a high-Mach-number interplanetary shock. We interpret the observed behavior as irregular "injections" of suprathermal particles resulting from shock front irregularities. Our findings, directly compared to self-consistent simulation results, provide important insights for the study of remote astrophysical systems where shock structuring is often neglected.

Unified Astronomy Thesaurus concepts: Interplanetary particle acceleration (826); Space plasmas (1544); Interplanetary shocks (829); Shocks (2086); Heliosphere (711)

1. Introduction

Collisionless shock waves are fundamental sources of energetic particles, which are ubiquitously present in our Universe and pivotal to explain many of its features, such as the nonthermal radiation emission common to many astrophysical sources, as revealed by decades of remote and direct observations (Reames 1999; Amato & Blasi 2018). Particle acceleration to suprathermal energies from thermal plasma, less understood than particle acceleration starting from an already energized population, remains a puzzle and has been the object of extensive theoretical and numerical investigations (Drury 1983; Caprioli & Spitkovsky 2014; Trotta et al. 2021).

Shocks in the heliosphere, unique as directly accessible by spacecraft (Richter et al. 1985), provide the missing link to remote observations of astrophysical systems. Direct observations of the Earth's bow shock using single- and multi-spacecraft approaches (e.g., Johlander et al. 2016) reveal a complex scenario of energy conversion and particle acceleration at the shock transition (Amano et al. 2020; Schwartz et al. 2022). The emerging picture, well supported by theory and modeling, is that small-scale irregularities in the spatial and temporal evolution of the shock environment (Greensadt et al. 1980; Matsumoto et al. 2015) are fundamental for efficient ion injection to high energies (Dimmock et al. 2019). This idea of irregular particle injection has been investigated in the past for the Earth's bow shock (Madanian et al. 2021) and in numerical simulations (Guo & Giacalone 2013), thus suggesting that particle behavior at shocks is much more complex than what is expected, neglecting spacetime irregularities, as suggested by early theoretical and numerical works (Decker 1990; Ao et al. 2008; Lu et al. 2009).

Such a complex picture is not as well observed and understood for shocks beyond the Earth's bow shock. In particular, shock structuring at interplanetary (IP) shocks, generated as a consequence of phenomena such as coronal mass ejections (Gosling et al. 1974) and its role in particle acceleration remains elusive (Blanco-Cano et al. 2016; Kajdič et al. 2019). IP shocks are generally weaker and have larger radii of curvature with respect to Earth's bow shock, allowing for direct observations of collisionless shocks in profoundly different regimes (e.g., Kilpua et al. 2015; Yang et al. 2020), and are more relevant to astrophysical environments such as galaxy cluster shocks, where shock irregularities are not resolved, but they are likely to play a crucial role in efficient particle acceleration (Brunetti & Jones 2014). Therefore, the study of particle injection at IP shocks is fundamental to test our current understanding built on Earth's bow shock, as well for addressing shocks at objects currently beyond reach. This paper demonstrates that, in order to address the suprathermal particle production upstream of supercritical collisionless shocks, the inherent variability of the injection process in both time and space must be taken into account.

The Solar Orbiter (SolO; Müller et al. 2020) mission probes the inner heliosphere with unprecedented levels of time-energy resolution for energetic particles, thus opening a new observational window for particle acceleration. In this work, we study the acceleration of low-energy (∼1 keV) particles to suprathermal energies (∼50 keV) at a strong IP shock observed by SolO at a heliocentric distance of about 0.8 au on 2021 October 30 at 22:02:07 UT. We use the Suprathermal Electrons and Protons (STEP) sensor of the Energetic Particle Detector (EPD) suite (Rodríguez-Pacheco et al. 2020), measuring particles in the 6–60 keV energy range (close to the injection range), at the very high time resolution of 1 s, close to suprathermal particle gyroscales. Our work exploits such novel, previously unavailable data sets for suprathermal particles upstream of IP shocks. We resolve upstream enhancements in the suprathermal particle population with dispersive velocity signatures and link them to
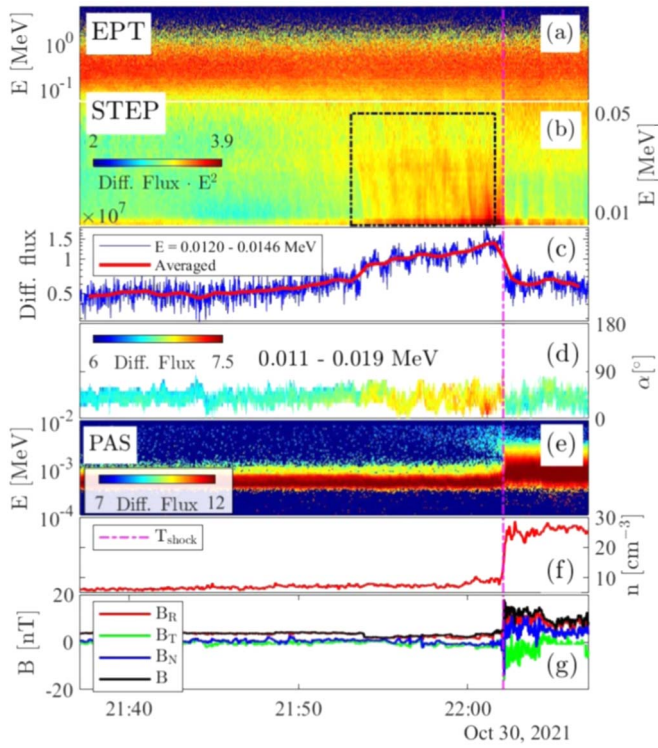
Figure 1. Event overview. (a) EPD-Electron Proton Telescope (EPT) particle flux (sunward aperture). (b) EPD-STEP particle flux (magnet channel averaged over the entire field of view). (c) Pitch-angle distributions for ions with an energy of 0.011–0.019 MeV in the spacecraft frame. (d) Time profile of the STEP energy flux in the 0.012–0.015 MeV energy channel at full resolution (blue) and time-averaged using a 1 minute window. (e) SWA-PAS ion energy flux (Owen et al. 2020). (f) SWA-PAS proton density. (g) MAG burst magnetic field data in Radial-tangential-normal (RTN) coordinates (Horbury et al. 2020). The magenta line marks the shock crossing, and the black rectangle in panel (b) highlights the dispersive energetic particle enhancements observed by STEP. Differential fluxes are in $E^2 \cdot \mathrm{cm}^{-2}\,\mathrm{s}^{-1}\,\mathrm{sr}^{-1}$ MeV for the EPD instruments and centimeters squared per second eV for PAS.

irregular proton injection along the shock front. Our findings are corroborated by kinetic simulations showing similar irregular proton energization upstream close to the shock, thus elucidating the mechanisms responsible for this behavior. This Letter is organized as follows: results are presented in Section 2. SolO observations are shown and discussed in Section 2.1, while modeling results are reported in 2.2. The conclusions are in Section 3.

2. Results

2.1. Solar Orbiter Observations

Figure 1 shows a 30 minute overview across the shock transition. Panels (a)–(b) reveal the presence of shock-accelerated particles at energies of up to 100 keV, while particle fluxes at higher energies do not respond to the shock passage. At these high energies, the fluxes were enhanced following a large solar energetic particle (SEP) event (see Klein et al. 2022).

The most striking feature of the period prior to the shock arrival at SolO is the irregular energetic particle enhancements particularly evident at 10–30 keV energies (Figure 1(b), black box), found in the time interval ∼15 minutes before the shock crossing, corresponding to 2×10^5 km or 2500 ion inertial lengths, d_i. These particle enhancements have the novel feature

of being dispersive in energy and are the focus of this work. The typical timescales at which the irregularities are observed are of 10–20 s, corresponding to spatial scales of about 50 d_i. Such signatures were previously inaccessible to observations, as shown in Figure 1(c), where the time profile of ion differential flux in the 0.012–0.015 MeV channel, rising exponentially up to the shock (Giacalone 2012), is shown at full resolution (blue) and averaged using a ∼1 minute window, typical of previous IP shock measurements. Figure 1(d) shows pitch-angle intensities for 0.011–0.019 MeV ions (i.e., energies at which the irregular enhancements are observed). Pitch angles are computed in the plasma rest frame assuming that all ions are protons and performing a Compton–Getting correction (Compton & Getting 1935), thereby combining magnetic field data from the magnetometer (MAG; Horbury et al. 2020), solar wind plasma data from the Proton and Alpha Particle Sensor (PAS) on the Solar Wind Analyser (SWA) instrument suite (Owen et al. 2020), and particle data from EPD/STEP (Yang et al. 2023). For the interval studied, low pitch angles are in the 30° field of view of STEP, relevant for shock-reflected particles. The irregular enhancements of energetic particles are field aligned, as is evident for the strongest signal close to the shock transition. The flux enhancement visible in PAS (Figure 1(e)) at lower energies starting immediately before the shock (22:00 UT) also reveals a field-aligned population. The study of the PAS low-energy population and the behavior very close to the shock transition is the object of another investigation (Dimmock et al. 2023).

The magnetic field reveals a wave foreshock ∼2 minutes upstream of the shock, in conjunction with a population of low-energy (∼4 keV) reflected particles seen by SWA/PAS, visible as the light blue enhancement in Figure 1(e) around 22:00 UT. Interestingly, the magnetic field is quieter where signals of irregular injection are found, indicating that efficient particle scattering may be reduced in this region (Lario et al. 2022). In this "quiet" shock upstream, we found two structures compatible with shocklets in the process of steepening (∼21:57 UT), very rarely observed at IP shocks (Wilson et al. 2009; Trotta et al. 2023a).

The shock parameters were estimated using upstream/downstream averaging windows varied systematically between 1 and 8 minutes (Trotta et al. 2022a). The shock was oblique, with a normal angle $\theta_{\mathrm{Bn}} = 44 \pm 1\overset{\circ}{.}5$ (obtained with the Mixed Mode 3 technique, MX3; Paschmann & Schwartz 2000), compatible with MX1,2 and magnetic coplanarity). The shock speed in the spacecraft frame and along the shock normal is $V_{\mathrm{shock}} = 400 \pm 5$ km s^{-1}. The shock Alfvénic and fast magnetosonic Mach numbers are $M_A \sim 7.6$ and $M_{\mathrm{fms}} \sim 4.6$, respectively. Thus, the event provides us with the opportunity to study a shock with particularly high Mach number in comparison with other IP shocks, while the shock speed is moderate with respect to typical IP shocks (Kilpua et al. 2015). The shock is supercritical and therefore expected to have a corrugated, rippled front (Trotta & Burgess 2019; Kajdic et al. 2021). The presence of reflected particles, enhanced wave activity in close proximity (1 minute) to the shock transition, and upstream shocklets in the process of steepening is consistent with the local shock parameters (Blanco-Cano et al. 2016).

To further elucidate the dispersive nature of the suprathermal particles, we show the STEP energy spectrogram in $1/v$ versus t space (Figure 2). Here, particle speeds are referred to the
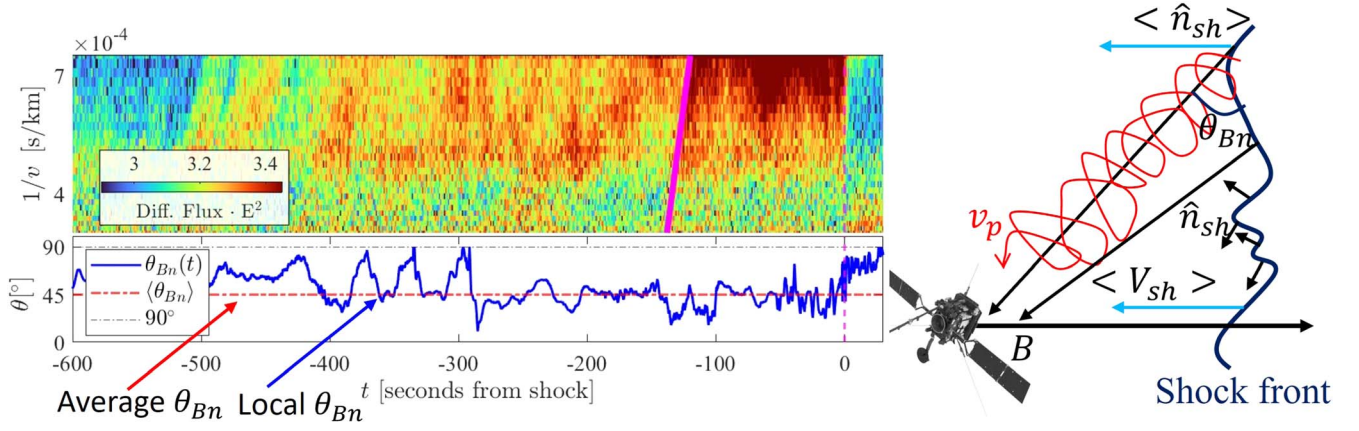
Figure 2. Left: spectrogram of the irregular signal in seconds from shock vs. $1/v$ axes, with the velocity dispersion shown by the solid magenta line (top). Time series showing the local $\theta_{\mathrm{Bn}}(t)$ angle. The red and gray dashed lines represent the average θ_{Bn} and a 90° angle, respectively (bottom). Right: cartoon showing the corrugated shock front with local shock normal, trajectory of a reflected particle ,and the SoLO trajectory (SoLO model: esa.com).[1]

center of the relative energy bin and computed in the spacecraft rest frame, assuming that all particles detected are protons (see Wimmer-Schweingruber & Pacheco 2021 for further details). During the period of irregular particle enhancements, we also combined magnetic field and plasma data to compute the particle pitch angles in the solar wind frame (Compton & Getting 1935), revealing that the particles detected by STEP are closely aligned with the field (not shown here). Interestingly, by visual inspection, it can be seen that these dispersive signals are shallower going far upstream, consistent with the fact that they are injected from more distant regions of the shock.

The dispersive flux enhancements are associated with irregular acceleration of protons along the shock front. Indeed, due to their dispersive nature, the particles detected by STEP cannot be continuously produced at the shock and propagated upstream, but they must come from a source that is only temporarily magnetically connected to the spacecraft due to time and/or space irregularities. Then, the fastest particles produced at the irregular source are detected first by the spacecraft, followed by the slower ones, yielding the observed dispersive behavior. Given the short timescales at which energetic particle enhancements are observed with respect to the shock and the quiet behavior of upstream magnetic field in the 10 minutes upstream of the shock, we assume that particles do not undergo significant scattering from their (irregular) production to the detection at SoLO. It is then natural to investigate the connection with the shock. The bottom left panel of Figure 2 shows the local $\theta_{\mathrm{Bn}}(t) \equiv \cos^{-1}(\mathbf{B}(t) \cdot \hat{\mathbf{n}}_{\mathrm{shock}}/|\mathbf{B}(t)|)$ changing significantly when the dispersive signals are observed, indicating that the spacecraft was indeed connected to different portions of the (corrugated) shock front, which in turn is expected to respond rapidly to upstream changes, as recent simulation work elucidated (e.g., Trotta et al. 2023b). Note that, given the single-spacecraft nature of the observations, the average shock normal computed with MX3 for both local and average θ_{Bn} estimation was used.

To further support this idea, similarly to velocity dispersion analyses (VDAs) used to determine the injection time of SEP events (e.g., Lintunen 2004; Dresing et al. 2023), we chose the clearest dispersive signal (~100 s upstream of the shock), and we superimpose the following relation (indicated by the magenta line in Figure 2):

$$t_{\mathrm{O}}(v) = t_i + \frac{s}{v}, \qquad (1)$$

where t_{O} represents the time at which the flux enhancement is observed for a certain speed v, t_i is the time of injection at the source, and s is the distance traveled by the particles from the source to the spacecraft. Thus, the argument is that the dispersive signals are due to accelerated particles produced by different portions of the shock front temporarily connected with the spacecraft, as sketched in Figure 2 (right). We note that, due to the very high energy-time resolution of STEP, it was possible to perform the VDA on such small (~seconds) timescales. Determining t_i based on the time when the highest energy particles are observed ($t_i \sim -130\,\mathrm{s}$), the source distance that we obtain through Equation (1) is $s \approx 4 \times 10^4$ km ($\sim 500 d_i$), compatible with their generation at the approaching shock, for which we would expect $s \sim V_{\mathrm{shock}} \Delta t / \sin(\theta_{\mathrm{Bn}})$, where V_{shock} is the average shock speed and Δt is the time delay between the observation of the dispersive signal and the shock passage. This is also compatible with the fact that the other dispersive signals observed farther upstream, such as the one before 21:54, about 500 s upstream of the shock (see Figure 2), show a shallower inclination though a more precise, quantitative analysis of this behavior is complicated by the high noise levels of the observation and will be the object of later statistical investigation employing more shock candidates (Yang et al. 2023).

2.2. Shock Modeling

Further insights about shock front irregularities are limited by the single-spacecraft nature of these observations. Therefore, we employ 2.5-dimensional kinetic simulations, with parameters compatible with the observed ones, to model the details of the shock transition, where proton injection to suprathermal energies takes place, relevant to our interpretation of the dispersive signals and enabling us to see how the shock surface and normal behave at small scales (see Figure 2). In the simulations, protons are modeled as macroparticles and advanced with the particle-in-cell method, while the electrons
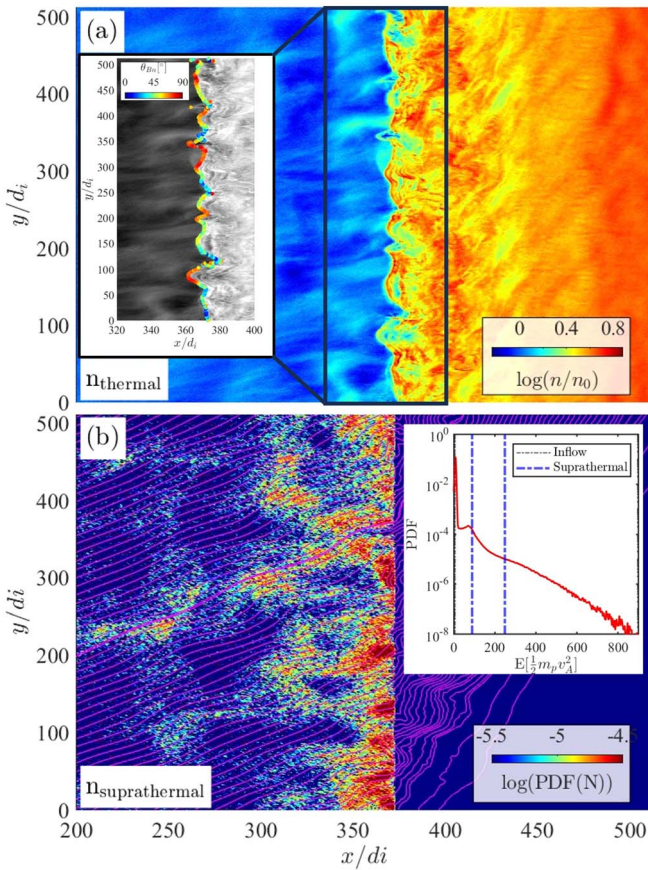
Figure 3. (a) Simulation snapshot of proton density (color map). The inset shows a zoom around the shock transition (gray), and the local shock position is superimposed, with a color map corresponding to the local θ_{Bn}. (b) Density map of upstream suprathermal protons (color map) and magnetic field lines (magenta) computed at the same simulation time as (a). The inset shows the upstream particle energy spectrum, with the dashed blue lines indicating the suprathermal energy range considered.

are modeled as a massless, charge-neutralizing fluid (Trotta et al. 2020).

In the model, distances are normalized to the ion inertial length d_i, times to the upstream inverse cyclotron frequency Ω_{ci}^{-1}, velocity to the Alfvén speed v_A, and the magnetic field and density to their upstream values B_0 and n_0. The shock is launched with the injection method (Quest 1985) where an upstream flow speed $V_{in} = 4.5 v_A$ was chosen, corresponding to $M_A \sim 6$. The shock nominal θ_{Bn} is 45°. The simulation domain is 512 d_i ×512 d_i, with resolution $\Delta x = \Delta y = 0.5\ d_i$ and a particle time step $\Delta t_{pa} = 0.01\ \Omega_{ci}^{-1}$. The number of particles per cell used is always greater than 300. This choice of parameters is compatible with the local properties of the IP shock as estimated from the SolO measurements. However, inherent variability routinely found in the simulations at small scales and in the observations at larger scales must be considered when comparing numerical and observational results. We note that these simulations are initialized with a laminar upstream, and therefore, the fluctuations that impact the shock are self-generated (due to particle reflection and subsequent upstream propagation). An exhaustive characterization of these self-induced fluctuations is discussed in Kajdic et al. (2021).

Simulation results are shown in Figure 3. In the top panel, we present the proton density for a simulation snapshot where the shock transition is well developed, showing the strongly perturbed character of the shock front. In such an irregular shock transition, particle dynamics become extremely complex (e.g., Lembege & Savoini 1992). To further elucidate the irregularities of the shock front, we computed the shock position in the simulation domain (with the criterion $B > 3B_0$, as in Trotta et al. 2023b) and evaluated the local θ_{Bn} along it (Figure 3(a), inset), showing high variability (see the cartoon in Figure 2).

In the bottom panel of Figure 3, we study the self-consistently shock-accelerated protons. The upstream energy spectrum is shown in the inset, with a peak at the inflow population energies and a suprathermal tail due to the accelerated protons. To address particle injection, we analyze the upstream spatial distribution of such suprathermal protons (Figure 3(b)) at the energies highlighted in the inset, which are a factor of 10 larger than the typical energies of particles in the upstream inflow population, in a similar fashion as the energy separation between the STEP energies at which the irregular enhancements are observed (~10 keV) and the solar wind population energies measured by PAS (~1 keV). It can be seen that suprathermal particles are not distributed uniformly, and their spatial distribution varies with their locations along the shock front, another indication of irregular injection. Further-more, we observed that the length scale of the irregularities is of 50 d_i, directly comparable with the irregularities seen in the STEP fluxes (see Figure 1). Higher energy particles also show irregularities.

3. Conclusions

We studied irregular particle acceleration from the thermal plasma using novel SolO observations. Particle injection to high energies is an extremely important issue for a large collection of astrophysical systems, making the SolO shock on 2021 October 30 an excellent event to tackle this interesting problem. The capabilities of the SolO EPD suite were exploited to probe the complex shock front behavior in the poorly investigated IP shock case. From this point of view, in situ observations of irregular particle enhancements have been used as a tool to address the (remote) structuring of the shock, information not available by simply looking at the spacecraft shock crossing at one point in space and time. Such an approach is reminiscent to the ones used to reconstruct the properties of SEP events (Krucker et al. 1999) and even to the ones looking at the properties of the heliospheric termination shock with the Interstellar Boundary Explorer mission (McComas et al. 2009), where particles produced at different portions of the shock are used to understand its dynamics (Zirnstein et al. 2022).

The hybrid kinetic simulations are consistent with this complex scenario of proton acceleration, with irregularly distributed suprathermal particles along the shock front, an invaluable tool to elucidate the small-scale behavior of this IP shock and of shock transitions in a variety of astrophysical systems. Our model highlights the very small-scale behavior of the shock but neglects other effects like preexisting turbulence and IP disturbances that may be important (Lario & Decker 2002; Trotta et al. 2022b; Nakanotani et al. 2022; Trotta et al. 2023b). The direct investigation of shock acceleration in systems other than the Earth's bow shock

---

(having a small radius of curvature and many other properties important for planetary bow shocks) is important to build a comprehensive understanding of collisionless shocks energetics. This work significantly strengthens an evolving theory of collisionless shock acceleration. Combining high-resolution energetic particle data upstream of heliospheric shocks with hybrid simulations, we have shown, for IP shocks, that the inherent variability of the injection process in both time and space must be considered to solve the problem of how suprathermal particle injection occurs in astrophysical systems. The process analyzed here is general, as it does not depend on how shock irregularities are generated. Indeed, this study is relevant for astrophysical systems where shock front irregularities cannot be resolved but are likely to play an important role for particle acceleration from the thermal distribution, such as galaxy cluster shocks, where efficient particle acceleration, which is inferred to happen at very large, $\sim$Mpc scales, remains a puzzle, particularly in the absence of preexisting cosmic rays (Botteon et al. 2020).

ORCID iDs

Domenico Trotta ● https://orcid.org/0000-0002-0608-8897
Timothy S. Horbury ● https://orcid.org/0000-0002-7572-4690
David Lario ● https://orcid.org/0000-0002-3176-8704
Rami Vainio ● https://orcid.org/0000-0002-3298-2067
Nina Dresing ● https://orcid.org/0000-0003-3903-4649
Andrew Dimmock ● https://orcid.org/0000-0003-1589-6711
Joe Giacalone ● https://orcid.org/0000-0002-0850-4233
Heli Hietala ● https://orcid.org/0000-0002-3039-1255
Robert F. Wimmer-Schweingruber ● https://orcid.org/0000-0002-7388-173X
Lars Berger ● https://orcid.org/0000-0001-7846-804X
Liu Yang ● https://orcid.org/0000-0002-6416-1538

References

Amano, T., Katou, T., Kitamura, N., et al. 2020, PhRvL, 124, 065101
Amato, E., & Blasi, P. 2018, AdSpR, 62, 2731
Ao, X., Zank, G. P., Pogorelov, N. V., & Shaikh, D. 2008, PhFl, 20, 127102
Blanco-Cano, X., Kajdič, P., Aguilar-Rodríguez, E., et al. 2016, JGRA, 121, 992
Botteon, Brunetti, G., Ryu, D., & Roh, S. 2020, A&A, 634, A64
Brunetti, G., & Jones, T. W. 2014, IJMPD, 23, 1430007
Caprioli, D., & Spitkovsky, A. 2014, ApJ, 783, 91
Compton, A. H., & Getting, I. A. 1935, PhRv, 47, 817
Decker, R. B. 1990, JGRA, 95, 11993
Dimmock, Gedalin, M., Lalti, A., et al. 2023, A&A, submitted
Dimmock, A. P., Russell, C. T., Sagdeev, R. Z., et al. 2019, SciA, 5, eaau9926
Dresing, N., Rodríguez-García, L., Jebaraj, I. C., et al. 2023, A&A, 674, A105
Drury, L. O. 1983, RPPh, 46, 973
Giacalone, J. 2012, ApJ, 761, 28
Gosling, J. T., Hildner, E., MacQueen, R. M., et al. 1974, JGR, 79, 4581
Greensadt, E. W., Russell, C., Gosling, J., et al. 1980, JGRA, 85, 2124
Guo, F., & Giacalone, J. 2013, ApJ, 773, 158
Horbury, T. S., O'Brien, H., Carrasco Blazquez, I., et al. 2020, A&A, 642, A9
Johlander, A., Vaivads, A., Khotyaintsev, Y. V., Retinó, A., & Dandouras, I. 2016, ApJL, 817, L4
Kajdic, P., Pfau-Kempf, Y., Turc, L., et al. 2021, JGRA, 126, e2021JA029283
Kajdič, P., Preisser, L., Blanco-Cano, X., Burgess, D., & Trotta, D. 2019, ApJL, 874, L13
Kilpua, E. K., Lumme, E., Andreeova, K., Isavnin, A., & Koskinen, H. E. 2015, JGRA, 120, 4112
Klein, K.-L., Musset, S., Vilmer, N., et al. 2022, A&A, 663, A173
Krucker, S., Larson, D. E., Lin, R. P., & Thompson, B. J. 1999, ApJ, 519, 864
Lario, D., & Decker, R. B. 2002, GeoRL, 29, 31
Lario, D., Richardson, I. G., Wilson, L. B. I., et al. 2022, ApJ, 925, 198
Lembege, B., & Savoini, P. 1992, PhFlB, 4, 3533
Lintunen, Vainio, R. 2004, A&A, 420, 343
Lu, Q., Hu, Q., & Zank, G. P. 2009, ApJ, 706, 687
Madanian, H., Schwartz, S. J., Fuselier, S. A., et al. 2021, ApJL, 915, L19
Matsumoto, Y., Amano, T., Kato, T. N., & Hoshino, M. 2015, Sci, 347, 974
McComas, D. J., Allegrini, F., Bochsler, P., et al. 2009, SSRv, 146, 11
Müller, St Cyr, O. C., Zouganelis, I., et al. 2020, A&A, 642, A1
Nakanotani, M., Zank, G. P., & Zhao, L.-L. 2022, ApJ, 926, 109
Owen, C. J., Bruno, R., Livi, S., et al. 2020, A&A, 642, A16
Paschmann, G., & Schwartz, S. J. 2000, in ESA Special Publication, ISSI Book on Analysis Methods for Multi-Spacecraft Data, ed. R. A. Harris, Vol. 449 (Paris: European Space Agency (ESA)), 99
Quest, K. B. 1985, PhRvL, 54, 1872
Reames, D. V. 1999, SSRv, 90, 413
Richter, A. K., Hsieh, K. C., Luttrell, A. H., Marsch, E., & Schwenn, R. 1985, Review of Interplanetary Shock Phenomena Near and within 1 AU, IN: Collisionless shocks in the heliosphere: Reviews of current research (Washington, DC: American Geophysical Union (AGU)), 33
Rodríguez-Pacheco, Wimmer-Schweingruber, R. F, Mason, G. M., et al. 2020, A&A, 642, A7
Schwartz, S. J., Goodrich, K. A., Wilson, L. B., III, et al. 2022, JGRA, 127, e2022JA030637
Trotta, D., & Burgess, D. 2019, MNRAS, 482, 1154
Trotta, D., Burgess, D., Prete, G., Perri, S., & Zimbardo, G. 2020, MNRAS, 491, 580
Trotta, D., Hietala, H., Horbury, T., et al. 2023a, MNRAS, 520, 437
Trotta, D., Pezzi, O., Burgess, D., et al. 2023b, MNRAS, 525, 1856
Trotta, D., Valentini, F., Burgess, D., & Servidio, S. 2021, PNAS, 118, e2026764118
Trotta, D., Vuorinen, L., Hietala, H., et al. 2022a, FrASS, 9, 1005672
Trotta, D., Pecora, F., Settino, A., et al. 2022b, ApJ, 933, 167
Wilson, L. B. I., Cattell, C. A., Kellogg, P. J., et al. 2009, JGRA, 114, A10106
Wimmer-Schweingruber, Janitzek, N. P., Pacheco, D., et al. 2021, A&A, 656, A22
Yang, L., Berger, L., Wimmer-Schweingruber, R. F., et al. 2020, ApJL, 888, L22
Yang, L., Heidrich-Meisner, V., Berger, L., et al. 2023, A&A, 673, A73
Zirnstein, E. J., Shrestha, B. L., McComas, D. J., et al. 2022, NatAs, 6, 1398